



Syntheses, structures and magnetic properties of Mn(II), Co(II) and Ni(II) metal–organic frameworks constructed from 1,3,5-benzenetricarboxylate and formate ligands

Ying Fu^a, Jie Su^a, Sihai Yang^b, Guobao Li^{a,*}, Fuhui Liao^a, Ming Xiong^c, Jianhua Lin^{a,*}

^a Beijing National Laboratory for Molecular Sciences (BNLMS), State Key Laboratory of Rare Earth Materials Chemistry and Applications, College of Chemistry and Molecular Engineering, Peking University, Beijing 100871, PR China

^b School of Chemistry, University of Nottingham, University Park, Nottingham NG7 2RD, UK

^c X-ray Laboratory, China University of Geoscience, Beijing 100083, PR China

ARTICLE INFO

Article history:

Received 19 August 2009

Received in revised form 10 November 2009

Accepted 13 November 2009

Available online 20 November 2009

Keywords:

Metal–organic framework

Carboxylate ligands

Magnetic property

Nickel

Manganese

Cobalt

ABSTRACT

Three compounds, $[(\text{CH}_3)_2\text{NH}_2][\text{M}_3(\text{BTC})(\text{HCOO})_4(\text{H}_2\text{O})]\cdot\text{H}_2\text{O}$ ($\text{M} = \text{Mn}$ (**1**), Co (**2**), Ni (**3**), $\text{H}_3\text{BTC} = 1,3,5$ -benzenetricarboxylic acid), were synthesized under hydrothermal conditions and were characterized by single crystal and powder X-ray diffraction, IR spectra, elemental analysis, coupled TG-MS and magnetic measurements. Compounds **1–3** are isostructural analogues and crystallize in monoclinic space group $P2_1/c$. Each metal ion in these compounds connects to six oxygen atoms to form a MO_6 octahedron. Six MO_6 octahedra link to each other to form a corner-shared hexameric M_6 cluster, which is linked by BTC ligands to form two-dimensional layers. The two-dimensional layers are further connected by formic ions to form a three-dimensional network with channels, where $(\text{CH}_3)_2\text{NH}_2^+$ ions and water molecular are located. Magnetic measurements indicate that anti-ferromagnetic ordering occurs at low temperature for these compounds.

© 2009 Elsevier B.V. All rights reserved.

1. Introduction

The design and synthesis of metal–organic frameworks (MOFs) on the basis of the assembly of metal ions and multifunctional organic ligands is a rapidly expanding research area due to their intriguing aesthetic structures and promising properties in gas adsorption, separation, catalysis, magnetism and nonlinear optics [1–12]. The construction of molecular architecture is influenced by the combination of several factors: medium, temperature, metal–ligand ratio, template, counterion and sometimes hydrogen bonding and π – π interactions [5,13–15]. The selection of metal ions and organic ligands is very important in the control of organic–inorganic frameworks in the self-assembly process [16–18]. Different ligands or metal ions have been used to synthesize MOFs with complex structures or multi-functions [19–23]. Such a trend has been followed by us, and several new results have been obtained. Here, we report the syntheses, structures and magnetic properties of metal–organic frameworks: $[(\text{CH}_3)_2\text{NH}_2][\text{M}_3(\text{BTC})(\text{HCOO})_4(\text{H}_2\text{O})]\cdot\text{H}_2\text{O}$ ($\text{M} = \text{Mn}$ (**1**), Co (**2**), Ni (**3**)), which adopt three-dimensional framework structures consisting of edge-sharing MO_6 octahedra with BTC and formate as ligands.

2. Experimental

2.1. Materials and characterizations

All solvents and reagents for the syntheses were of analytical grade and were used as received from commercial sources without further purification. Powder X-ray diffraction data of the studied samples were collected on a Rigaku D/Max-2000 diffractometer with $\text{Cu K}\alpha$ radiation ($\lambda = 1.5418 \text{ \AA}$) at 40 kV, 100 mA and a graphite monochromator at the secondary beam. Magnetic data of polycrystalline samples were measured on a Quantum Design MPMS-5S SQUID Spectrometer in the 2–300 K temperature range. Correction for the sample holder was applied. IR spectra were recorded on a Magna-IR 750 FTIR spectrophotometer in the region of 4000 – 650 cm^{-1} . Elemental analyses for C, H and N were carried out on Elementar Vario EL III microanalyzer. TG-MS analyses were performed in air atmosphere with a heating rate of $10 \text{ }^\circ\text{C}/\text{min}$ from 50 to $800 \text{ }^\circ\text{C}$, using a NETZSCH STA449C instrument. Electron paramagnetic resonance (EPR) spectrums of the studied samples were recorded on a powdered sample at X band at 300 K on the Bruker ESP300 Electron Spin Resonance Spectrometer.

2.2. Syntheses

Identical synthetic procedures were used to prepare the three compounds. To synthesize **1**, a mixture of $\text{MnCl}_2\cdot 4\text{H}_2\text{O}$ (3.0 mmol,

* Corresponding authors. Tel.: +86 10 62750342; fax: +86 10 62753541 (G. Li).
E-mail addresses: liguobao@pku.edu.cn (G. Li), jhlin@pku.edu.cn (J. Lin).

0.5937 g), H₃BTC (1.0 mmol, 0.2101 g), DMF (*N,N*-dimethylformamide) (5.0 ml) and distilled water (5.0 ml) was placed in a 23 ml Teflon-lined stainless autoclave. The autoclave was sealed, heated to 120 °C at a rate of 10 °C/h, kept at 120 °C under autogenous pressure for 5 days, and then cooled to room temperature at a rate of 5 °C/h. Colorless crystals were filtered, washed with DMF and distilled water and then dried in air to give about 0.53 g of **1** (yield 84% based on H₃BTC). The (CH₃)₂NH₂⁺ and HCOO⁻ were generated via decomposition of DMF. *Anal. Calc.* for C₁₅H₁₉NO₁₆Mn₃ (Fw: 634.13): C, 28.41; H, 3.02; N, 2.21. Found: C, 28.42; H, 2.69; N, 2.17%.

The cobalt analogue **2** was prepared by an identical procedure to that described for **1**, and then purple crystals were obtained (yield 73% based on H₃BTC). *Anal. Calc.* for C₁₅H₁₉NO₁₆Co₃ (Fw: 646.10): C, 27.88; H, 2.96; N, 2.17. Found: C, 27.76; H, 2.64; N, 2.08%. The nickel analogue **3** was prepared as light green crystals (yield 71% based on H₃BTC) using the similar procedure as that for **1**. *Anal. Calc.* for C₁₅H₁₉NO₁₆Ni₃ (Fw: 645.44): C, 27.91; H, 2.97; N, 2.17. Found: C, 27.64; H, 3.17; N, 2.27%.

2.3. Crystallographic studies

Suitable single crystals of **1**, **2** and **3** were carefully selected under an optical microscope and glued to thin glass fibers with epoxy resin. X-ray single-crystal diffraction data of **1** and **2** were collected

Table 1
Crystallographic data and structural refinement parameters for **1–3**.

	1	2	3
Formula	C ₁₅ H ₁₉ NO ₁₆ Mn ₃	C ₁₅ H ₁₉ NO ₁₆ Co ₃	C ₁₅ H ₁₉ NO ₁₆ Ni ₃
Formula weight	634.13	646.10	645.44
T (K)	298(2)	298(2)	120(2)
Space group	P2 ₁ /c	P2 ₁ /c	P2 ₁ /c
a (Å)	9.756(2)	9.616(2)	9.540(2)
b (Å)	14.139(3)	13.904(3)	13.783(3)
c (Å)	15.733(3)	15.346(3)	15.154(3)
β (°)	90.96(3)	91.18(3)	91.02(3)
V (Å ³)	2170.0(8)	2051.4(7)	1992.2(7)
Z	4	4	4
D _{calc} (g cm ⁻³)	1.941	2.092	2.152
λ (Mo Kα) (Å)	0.71073	0.71073	0.71073
μ (mm ⁻¹)	1.803	2.487	2.898
Goodness-of-fit on F ²	1.000	1.002	1.001
R _{int}	0.0454	0.0538	0.0520
R ₁ , wR ₂ [I > 2σ (I)]	0.0613, 0.1659	0.0379, 0.1159	0.0421, 0.1435
R ₁ , wR ₂ (all data)	0.0666, 0.1713	0.0458, 0.1233	0.0536, 0.1576

Table 2
Selected bond distances (Å) for **1–3**.

Bond	1 (M = Mn)	2 (M = Co)	3 (M = Ni)
M1–O3	2.136(3)	2.052(2)	2.022(3)
M1–O5	2.194(3)	2.136(2)	2.093(3)
M1–O8	2.194(3)	2.091(3)	2.069(3)
M1–O11	2.194(3)	2.091(3)	2.051(3)
M1–O13	2.226(3)	2.133(2)	2.090(3)
M1–O15	2.184(3)	2.108(2)	2.067(3)
M2–O1	2.137(3)	2.085(2)	2.054(3)
M2–O4	2.184(3)	2.085(2)	2.042(3)
M2–O6	2.176(3)	2.104(3)	2.074(3)
M2–O9	2.225(3)	2.134(2)	2.084(3)
M2–O12	2.199(3)	2.133(2)	2.074(3)
M2–O13	2.175(3)	2.079(2)	2.041(3)
M3–O2	2.172(3)	2.103(2)	2.077(3)
M3–O7	2.200(3)	2.118(3)	2.061(3)
M3–O9	2.199(3)	2.100(2)	2.062(3)
M3–O10	2.203(3)	2.134(2)	2.096(3)
M3–O11	2.210(3)	2.124(2)	2.073(3)
M3–O14	2.118(3)	2.035(2)	2.000(3)

on a Rigaku AFC6S diffractometer by using the ω-2θ scan method at room temperature. Their PSI absorption corrections were applied using the TEXSAN program [24]. The intensity data of **3** were collected at 120 K on a Bruker NONIUS X-ray diffractometer, equipped with an APEX-CCD area detector. The data absorption correction of **3** was applied using the SADABS program [25]. The structures were solved by the direct method and refined on F² with full-matrix least-squares methods using the SHELXS-97 and SHELXL-97 programs, respectively [26]. All of the non-hydrogen atoms were refined anisotropically. Hydrogen atoms were added in the riding model and refined isotropically with O–H = 0.82 Å, N–H = 0.90 Å and C–H = 0.93 Å (in BTC or formate) or C–H = 0.96 Å (in (CH₃)₂NH₂⁺). The crystallographic data and structural refinement parameters are presented in Table 1, and the selected bond lengths are listed in Table 2.

3. Results and discussion

3.1. Infrared (IR) spectra

FT-IR spectra of these compounds are shown in Fig. 1. The broad absorption bands of the asymmetric and symmetric stretching vibrations of water appear at 3612–3081 cm⁻¹ [13,27–29]. The bands at 1650–1547 cm⁻¹ and 1442–1336 cm⁻¹ correspond to the asymmetric and symmetric stretching vibrations of the bound carboxylic groups (CO₂M), respectively [13,27–31]. And the bands at 863–807 cm⁻¹ and 798–714 cm⁻¹ are related to the stretching vibrations of C–C groups and the out-of-plane deformation vibrations of the C–H groups in the benzene ring [27–29]. The absence of the absorption bands from 1680–1800 cm⁻¹ indicates the complete deprotonation of BTC ligands [30]. A group of bands at 2917–2779 cm⁻¹ is due to the asymmetric and symmetric stretching vibrations of H₂N⁺ groups.

3.2. Crystal structure

Compounds **1–3** are isostructural analogues with slight differences in the lattice parameters. They crystallize in the monoclinic space group P2₁/c. Here **1** is taken as an example to present and discuss the structure in detail. In the asymmetric unit of **1** (Fig. 2a), there are three crystallographic independent Mn(II) ions (Mn(1), Mn(2) and Mn(3)), one BTC ligand, four formate ligands, one terminal water molecule, one (CH₃)₂NH₂⁺ ion, and one free water molecular. Each Mn(II) ion is six coordinated to form a distorted octahedron with Mn–O bond distances in the range of 2.118–2.225 Å and O–Mn–O angles from 83.51° to 98.63° or 168.30° to 176.64°. The Mn(1) ion is coordinated with two carboxyl oxygen atoms (O3, O5) from two BTC ligands, three carboxyl oxygen atoms (O11, O13, O15) from formate ligands in a 3.21 (*syn, syn, anti*) mode [32–34] (here, the symbol “(n + m).nm (*syn* or *anti, syn* or *anti, anti* or *syn*)”, means that (n + m) metal ions link to a formate, n metal ions connect to one oxygen atom of the formate, and m metal ions connect to the another oxygen atom of the formate; *syn* or *anti* means the mode of the connection of a metal ion to the formate is *syn* or *anti*), and one oxygen atom (O8) from a terminal water molecule. The Mn(2) ion is bound with two BTC (O1, O4), three 3.21 (*syn, syn, anti*) formates (O9, O12, O13) and one 2.11 (*anti, anti*) formate (O6). The Mn(3) ion links with two BTC linkers (O2, O14), three 3.21 (*syn, syn, anti*) formates (O7, O9ⁱⁱ, O11) and one 2.11 (*anti, anti*) formate (O10).

In **1**, each bridging BTC is completely deprotonated, binding to six separate Mn(II) ions. The formates have two bridging modes: the 2.11 (*anti, anti*) and the 3.21 (*syn, syn, anti*) bridging configurations. By the six carboxyl oxygen atoms of the 3.21 (*syn, syn, anti*) formates, six MnO₆ octahedra link to each other to form a corner-

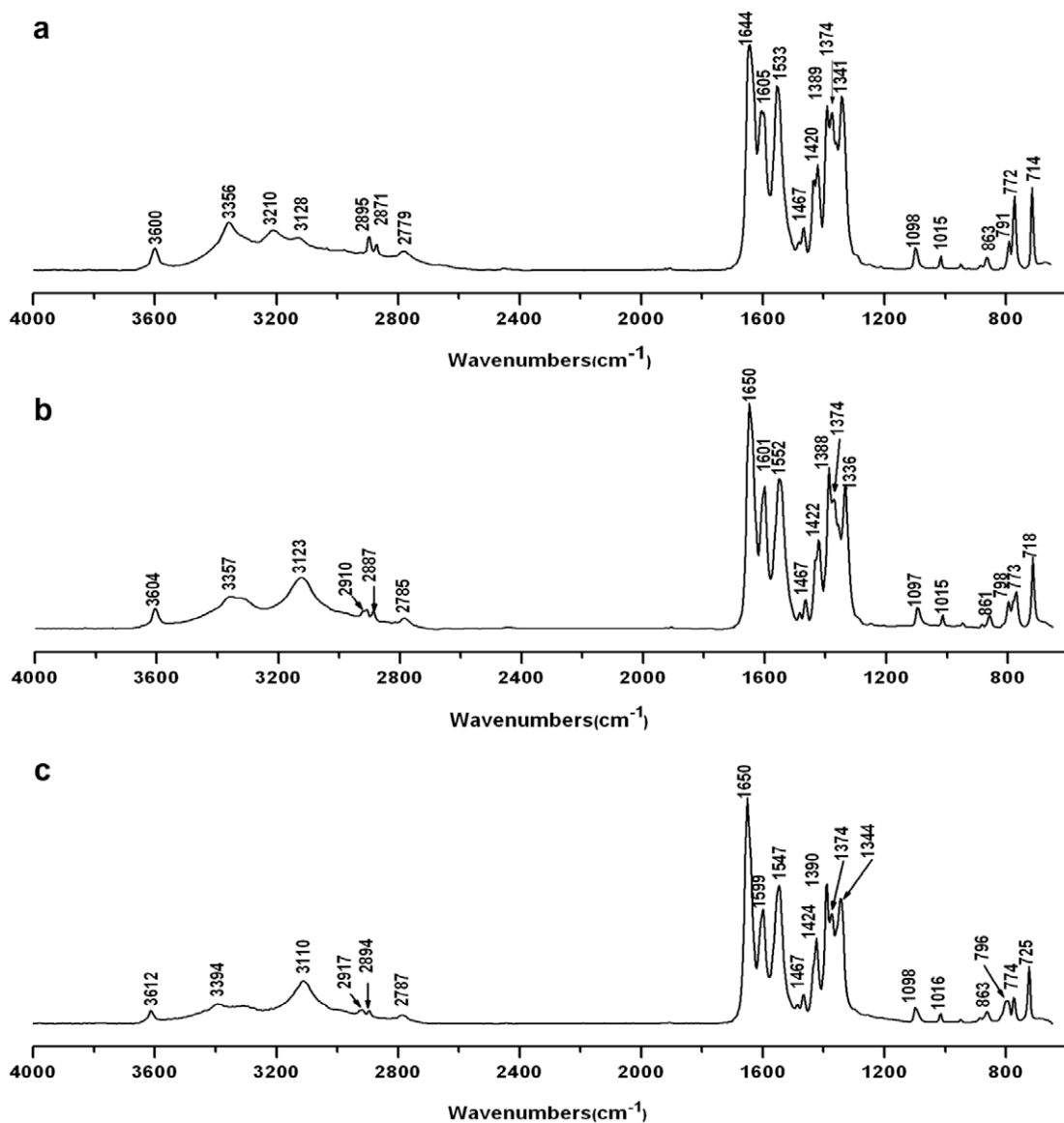


Fig. 1. FTIR spectra of (a) **1**, (b) **2** and (c) **3**.

shared hexameric Mn_6 cluster, which is shown in Fig. 2b. Those Mn_6 clusters are connected together via BTC bridges to form a two-dimensional layer stacking along [1 0 2] (Fig. 2c), which is similar to MOF-CJ4 [30]. Further, these two-dimensional parallels are bridged by the 2.11 (*anti*, *anti*) formates to assemble a three-dimensional (3D) network (Fig. 2d). To our knowledge, such a kind of structure, consisting of hexanuclear clusters [30,31,35,36], two different bridging modes (3.21 and 2.11) of formates and one type BTC linkers, has not been found in polymeric frameworks before.

The projections of the 3D network of **1** along different axes are shown in Fig. 3. When seeing along the *c*-axis, free water molecules (only oxygen atoms are shown) are found to be isolated from the 3D network as shown in the left plot of Fig. 3. This means that there are channels along the *c*-axis, where free water molecules can be located. However, no $(CH_3)_2NH_2^+$ ions are found in these channels. Similarly, there are channels along the *b*-axis, where $(CH_3)_2NH_2^+$ ions and free water molecules can be found as shown in the middle plot of Fig. 3. As shown in the right plot of Fig. 3, when seeing along the *a*-axis, part of the $(CH_3)_2NH_2^+$ ion can be seen in the channels, part is buried in the wall of channels. Therefore, the channels in **1**

are two-dimensional for free water molecule, and one-dimensional for $(CH_3)_2NH_2^+$ ions.

3.3. Thermal properties

The TG data of the compounds under an air atmosphere are obtained at a heating rate of 10 °C/min, which are shown in Fig. 4a. Similar thermal behavior is observed. The analogues lose the free and the coordinated water molecules at 80–200 °C (Calc. 5.68 wt%, Found 5.50 wt%) for **1**, at 130–230 °C (Calc. 5.58 wt%, Found 5.26 wt%) for **2** and at 120–260 °C (Calc. 5.58 wt%, Found 6.17 wt%) for **3**. The MS spectra (Fig. 4) show peaks at these temperature only for ions with $m/z = 16, 17$ and 18 , which may be assigned to O^+ , HO^+ and H_2O^+ , respectively. Compounds **1** and **3** decompose the organic parts in two steps, while **2** lose such weight at one step. The measured weight loss is about 56.38 wt% (Calc. 56.98 wt%) at 200–400 °C for **1**, 56.84 wt% (Calc. 55.91 wt%) at 230–350 °C for **2**, and 58.88 wt% (Calc. 59.70 wt%) at 260–410 °C for **3**. The MS peaks of ions with $m/z = 15, 30, 44, 45$ and 46 are observed during the above decomposition, which may correspond to

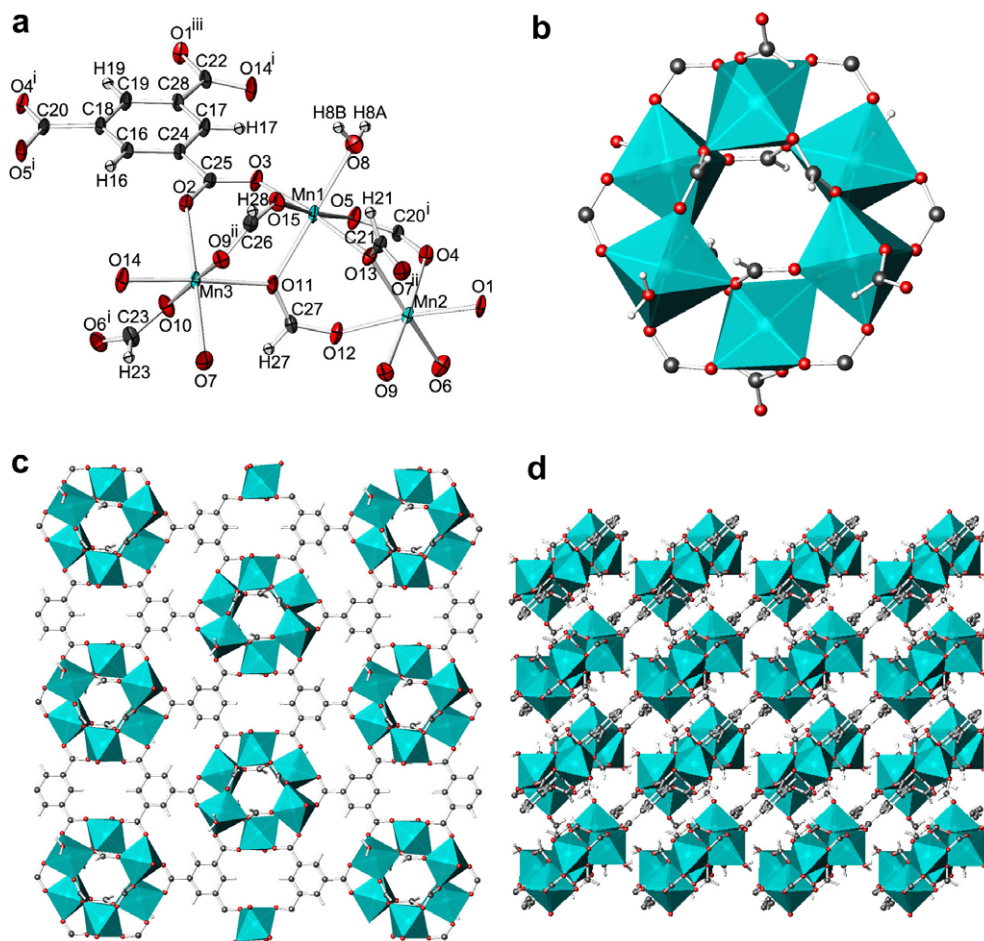


Fig. 2. The structure details of **1**. (a) Thermal ellipsoid plot (50%) drawing of the coordination environment of Mn(II) ions, symmetry code: (i) $-x, y + 1/2, -z + 1/2$; (ii) $-x, -y, -z$; (iii) $x, -y + 1/2, z + 1/2$; (b) The hexameric Mn_6 cluster; (c) The two-dimensional layer with hexameric Mn_6 clusters linked together via BTC ligands viewed along $[1\ 0\ 2]$; (d) Projection view along $[0\ 1\ 0]$, showing the three-dimensional framework with two-dimensional layers linked together via the 2.11 (*anti, anti*) formate ligands. (Color code: Mn, cyan; C, grey; O, red; H, white; MnO_6 octahedron, cyan). (For interpretation of the references to colour in this figure legend, the reader is referred to the web version of this article.)

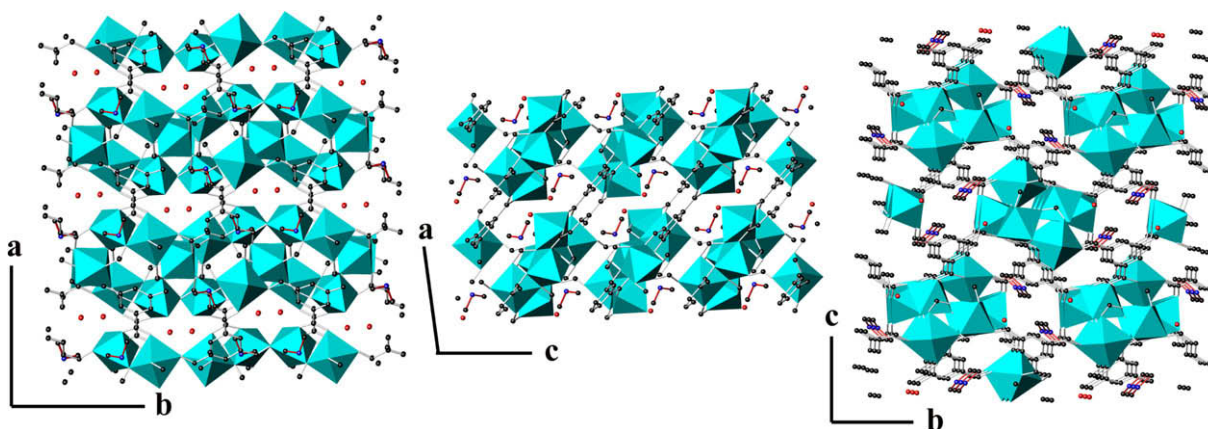


Fig. 3. The projections of the three-dimensional network of **1** along different axes. Hydrogen atoms are omitted. (Color code: C, grey; O, red; N, blue; MnO_6 octahedron, cyan). (For interpretation of the references to colour in this figure legend, the reader is referred to the web version of this article.)

CH_3^+ or NH^+ , NO^+ or CH_3NH^+ , CO_2^+ or $(CH_3)_2N^+$, $HCOO^+$ or $(CH_3)_2NH^+$, NO_2^+ or $(CH_3)_2NH_2^+$, respectively. The final residual weights are about 38.12 wt% (Calc. 37.34 wt%) of **1**, 37.90 wt% (Calc. 37.27 wt%) of **2** and 34.95 wt% (Calc. 34.72 wt%) of **3**, which agree well with the decomposition products Mn_2O_3 (PDF#41-

1442), Co_3O_4 (PDF#43-1003) and NiO (PDF#47-1049), confirmed by powder X-ray diffraction patterns shown in Fig. 5a. In addition, powder X-ray diffraction patterns of **1–3** treated at different temperatures are presented in Fig. 5b–d, respectively. It is found that there are almost no changes in the powder X-ray diffraction pat-

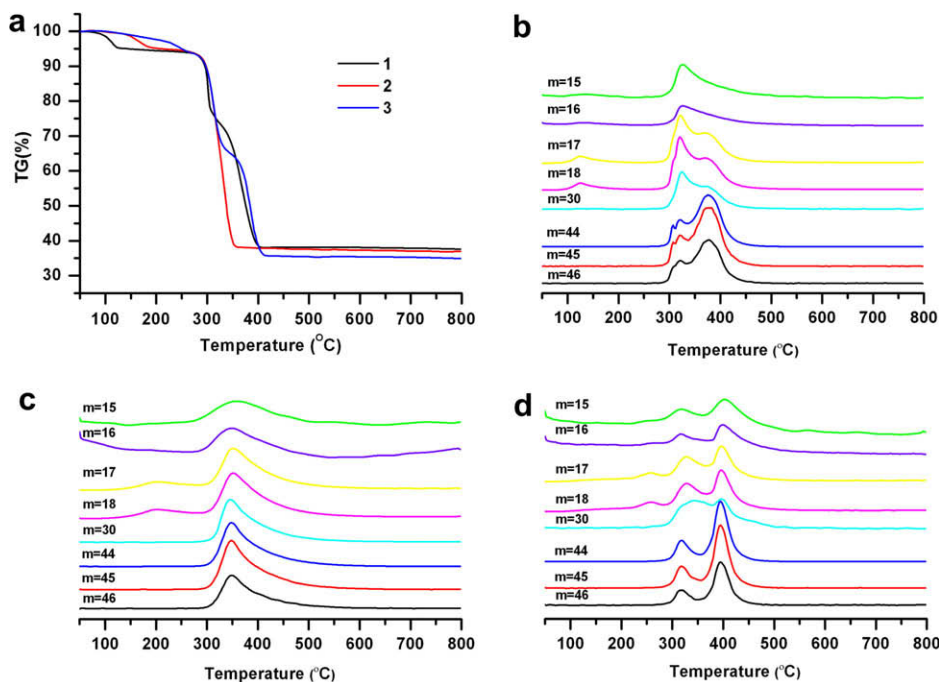


Fig. 4. (a) TG curves of 1–3, (b) MS curves of 1, (c) MS curves of 2, (d) MS curves of 3.

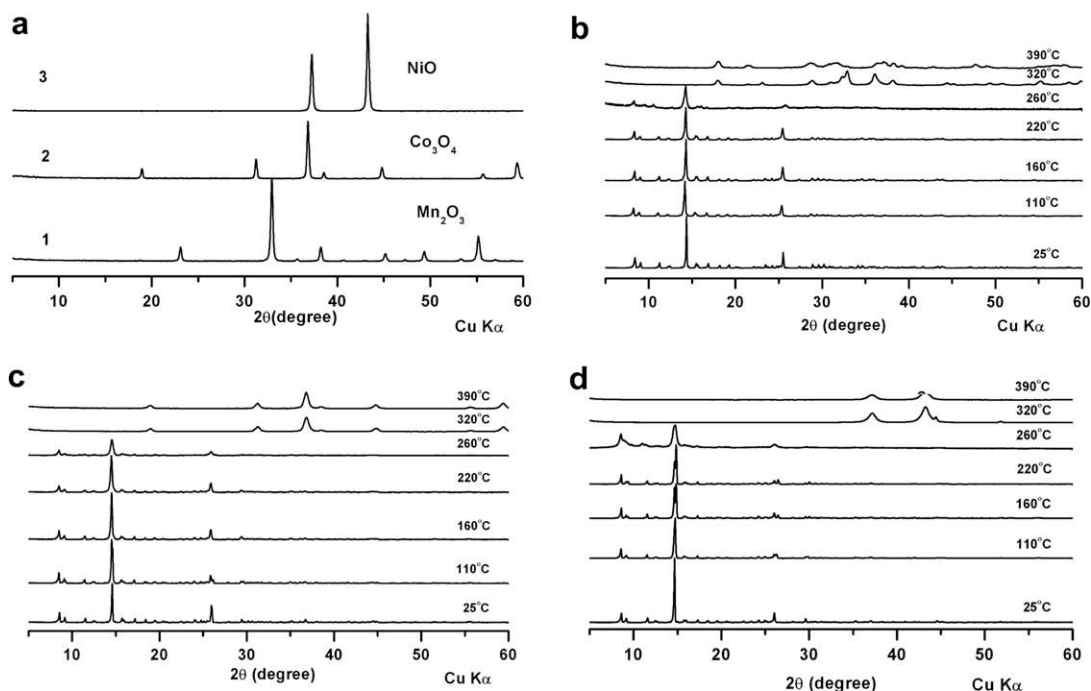


Fig. 5. (a) Powder X-ray diffraction patterns of the final residual of 1, 2 and 3 after TG-MS progress in an air atmosphere; (b) powder X-ray diffraction patterns of 1 treated at different temperatures; (c) powder X-ray diffraction patterns of 2 treated at different temperatures; (d) powder X-ray diffraction patterns of 3 treated at different temperatures.

terns of 1–3 when the treated temperature is between 25 and 220 °C. When the treated temperature is about 260 °C, the diffraction patterns become apparently weak and broad with some small peaks corresponding to unknown phases. When the treated temperature is above 320 °C, the diffraction patterns for 1 are due to Mn_5O_8 (PDF#39-1218), the diffraction patterns for 2 are attributed to Co_3O_4 (PDF#43-1003). The diffraction patterns for 3 are attributed to NiO (PDF#47-1049) and Ni (PDF#65-2865) when the

treated temperature is about 320 °C, and are due to NiO (PDF#47-1049) when the treated temperature is about 390 °C. Therefore, the above results suggest that 1–3 are stable up to 220 °C.

3.4. EPR and magnetic properties

EPR data at 300 K for 1 and 2 are obtained and shown in Fig. 6, from which the g values for Mn^{+2} ($g = 2.008(2)$) and Co^{+2}

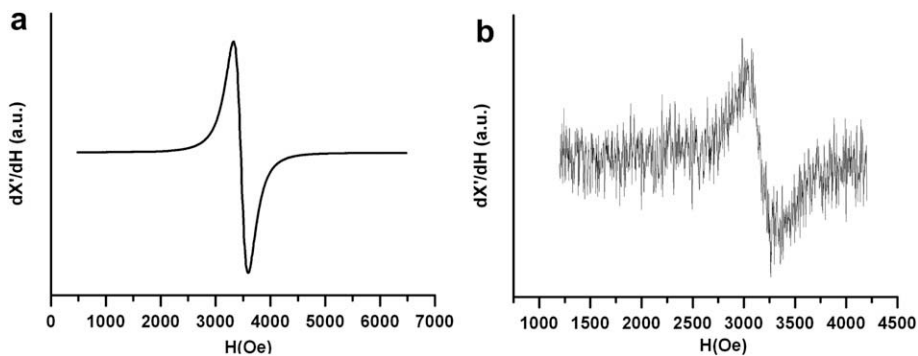


Fig. 6. EPR signals at 300 K for **1** (a) and **2** (b).

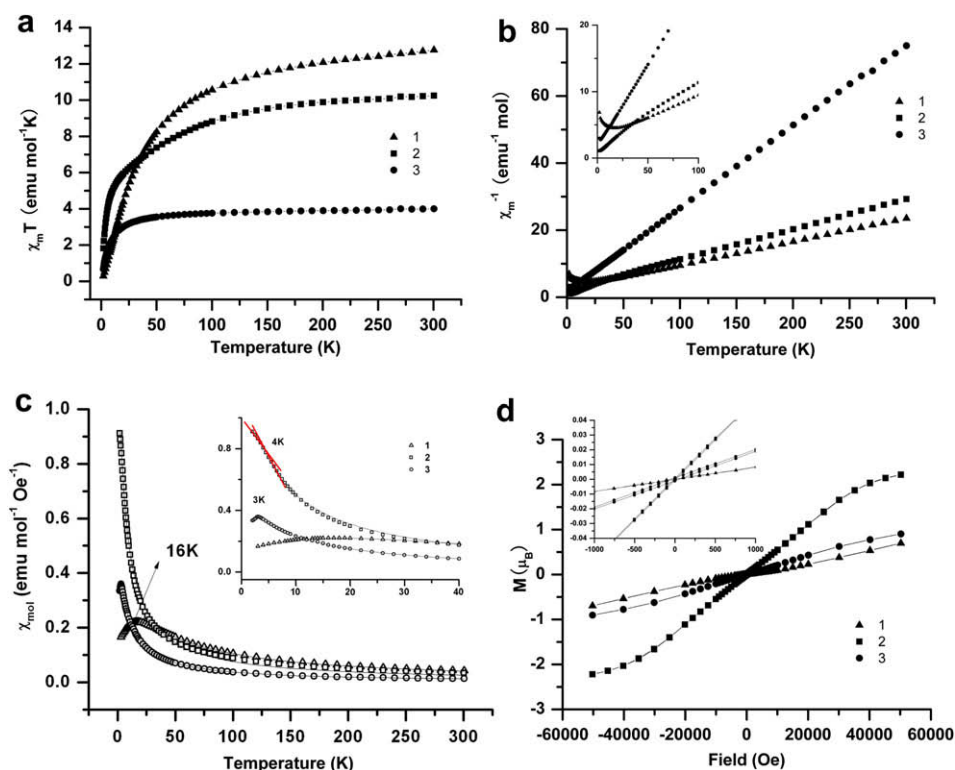


Fig. 7. Temperature dependence of (a) $\chi_m T$, (b) χ_m^{-1} , and (c) χ_m , and (d) field dependence of M at 2 K of **1**, **2** and **3**. The solid lines in (c) are the fitting results from Eq. (4), the corresponding parameters are listed in Table 3.

($g = 2.215(2)$) are observed. No EPR signal is observed for **3** because the electrons in Ni^{+2} of **3** are paired.

The magnetic susceptibility measured from 2 to 300 K at 1000 Oe for **1**, **2** and **3**, are displayed in Fig. 7. The values of $\chi_m T$ at 300 K for **1** and **3** are 12.76 and 4.00 $\text{emu mol}^{-1} \text{K}$, respectively, which are as expected for three “isolated” Mn(II) ions and Ni(II) ions [37–39]. The value of $\chi_m T$ at 300 K for **2** is 10.24 $\text{emu mol}^{-1} \text{K}$ (the corresponding effective magnetic moment per Co(II) $\mu_{\text{eff}} = 5.22 \mu_{\text{B}}$), which is much higher than that expected for three “isolated” Co(II) ions ($\chi_m T = 5.63 \text{emu mol}^{-1} \text{K}$ for three “isolated” $S = 3/2$ ions), indicating relatively strong spin-orbit coupling [40]. This is very typical for octahedrally coordinated Co(II) ion with $^4T_{1g}$ electronic state, for which the observed moments typically fall in the range 4.3–5.2 μ_{B} [41,42].

The magnetic susceptibility above 50 K can be well fit to the Curie–Weiss law with Curie constants $C = 14.20$, 11.15 and 4.08 $\text{emu mol}^{-1} \text{K}$ and Weiss constant $\theta = -35.0$, -26.3 and -8.6K for

1–3, respectively. The negative θ values indicate the presence of anti-ferromagnetic interactions between Mn(II), Co(II) or Ni(II) ions. It is easy to find from the χ_m-T curves shown in Fig. 7c that the Néel temperatures of **1** and **3** are 16 K and 3 K, respectively. However, it is a little difficult to find the Néel temperature of **2**. A change in slope of the χ_m-T curve is observed at 4 K, which is suggested to be the Néel temperature of **2** following this method after Goff et al. [43].

Weak magnetic loops are observed for **2** and **3** at 2 K (Fig. 7d). This behavior can be caused by ferro- or ferri-magnetic moment, or canted anti-ferromagnetic moment. And the above discussions have already shown that magnetic interactions in **2** and **3** are anti-ferromagnetic. Therefore, it is reasonable to suggest the magnetic moment of **2** and **3** are canted at lower temperature.

As shown in Fig. 8, the magnetic networks of **1–3** are two-dimensional and can be divided into chains shown by the black lines. Because the M2 and M3 sites are very similar, and the lengths

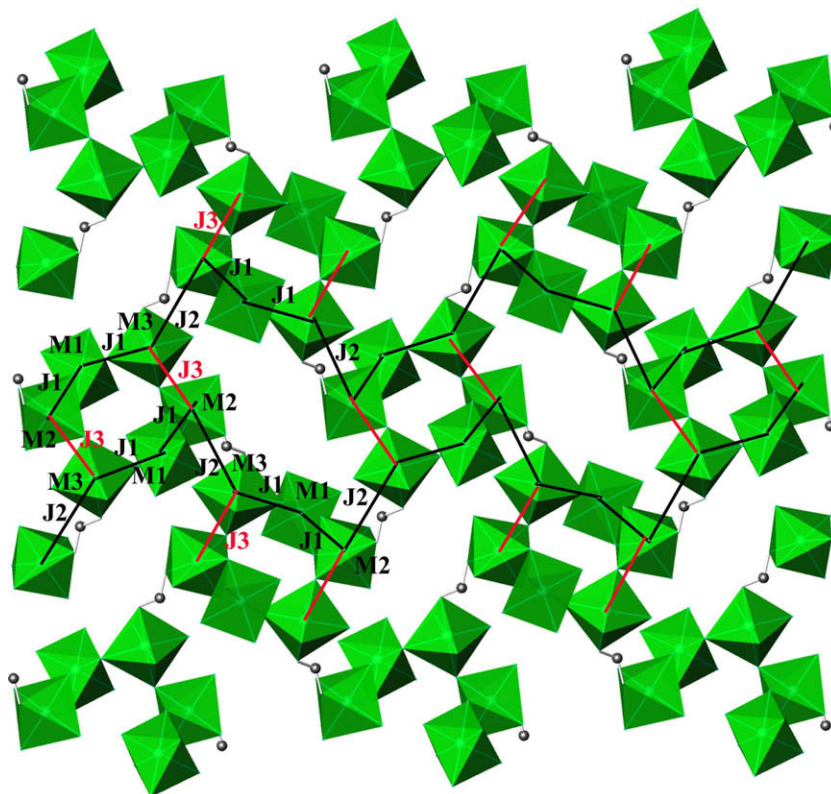


Fig. 8. Magnetic model for **1**, **2** and **3**.

of M1–M2 (3.68 Å for M = Mn) and M1–M3 (3.65 Å for M = Mn) are almost equal, the same exchange interaction J_1 is supposed for M1–M2 and M1–M3. The exchange interaction between M2 and M3 connected by formic ions is set to J_2 . After these approximations, the chains can be treated as the $J_1J_1J_2$ magnetic chains. The bulk susceptibility of such a chain has been suggested as below by Abu-Youssef et al. [44]

$$\chi = \frac{N_A g^2 \mu_B^2 S(S+1) \{3 + 2\mu_2 + 4\mu_1(1 + \mu_2) + \mu_1^2(2 + 3\mu_2)\}}{3k_B T(1 - \mu_1^2 \mu_2)} \quad (1)$$

$$\mu_p = \coth(J_p/k_B T) - k_B T/J_p \quad (p = 1, 2) \quad (2)$$

where χ is the magnetic susceptibility, N_A the Avogadro constant, k_B the Boltzmann constant, μ_B the Bohr magneton, T the temperature (K), g the g factor, S the classical spin vector.

The exchange interaction between the chains is set as J_3 . To simplify the consideration of the contribution of the inter-chain interactions, the detail structure of the chain can be firstly omitted, and then a model of 1D Heisenberg anti-ferromagnet consisting of interactions $J_3J_3J_3$ can be used to describe the magnetic contribution of the inter-chain interactions. In this case, the bulk susceptibility has been suggested as below by Fisher [45]

$$\chi = \frac{N_A g^2 \mu_B^2 S(S+1)}{3k_B T} \times \frac{1 + \mu_3}{1 - \mu_3} \quad (3)$$

Here μ_3 represented the magnetic interaction between the chains. After combined the contribution within the chain and inter-chains, the bulk susceptibility could be suggested as below [46]

$$\chi = \frac{N_A g^2 \mu_B^2 S(S+1) \{3 + 2\mu_2 + 4\mu_1(1 + \mu_2) + \mu_1^2(2 + 3\mu_2)\}}{3k_B T(1 - \mu_1^2 \mu_2)} \times \frac{1 + \mu_3}{1 - \mu_3} \quad (4)$$

Table 3
Magnetic fitting results for **1**, **2** and **3**.

M	g	J_1 (cm ⁻¹)	J_2 (cm ⁻¹)	J_3 (cm ⁻¹)
Mn	2.030(9)	-21.6(3)	-33.0(4)	-0.64(5)
Co	2.371(8)	4.21(2)	-20.5(2)	0.08(1)
Ni	2.289(8)	3.24(8)	-17.8(2)	-1.00(4)

The above model provides a good description of the susceptibility in all temperature ranges for **1**, **2** and **3** as shown in Fig. 7c. The corresponding values for g 's and J 's are listed in Table 3. The obtained values of g for **1**, **2** and **3**, are similar to that reported [47–49]. In addition, the g values for **1** and **2** agree well with the measured values by EPR. The dominant minus value for J 's agrees well with major anti-ferromagnetic interactions found in these compounds. However, it is just one possible explanation for the magnetic data. More data from neutron diffraction data and other studies are needed to give a full understanding for the magnetic behavior of these compounds.

4. Conclusion

The combination of the aromatic BTC ligands and formate to react with transition metals affords three three-dimensional metal–organic frameworks through hydrothermal synthesis. Fully deprotonated BTC ligands link hexameric M_6 clusters of six vertexes-shared MO_6 octahedra bridged by 3.21 (*syn*, *syn*, *anti*) formates to form two-dimensional parallels. Furthermore, such parallels are connected by the 2.11 formates with the (*anti*, *anti*) modes to construct a three-dimensional network containing $(CH_3)_2NH_2^+$ and H_2O guests. At low temperature, **1–3** are antiferromagnets.

Acknowledgement

This work is supported by the National Natural Science Foundation of China (Grants 20771008, 2073116003 and 20821091).

Appendix A. Supplementary material

CCDC 724746, 724747 and 724748 contain the supplementary crystallographic data for compounds 1–3. These data can be obtained free of charge from The Cambridge Crystallographic Data Centre via www.ccdc.cam.ac.uk/data_request/cif. Supplementary data associated with this article can be found, in the online version, at doi:10.1016/j.ica.2009.11.019.

References

- [1] O.M. Yaghi, H.L. Li, C. Davis, D. Richardson, T.L. Groy, *Acc. Chem. Res.* 31 (1998) 474.
- [2] S.R. Batten, R. Robson, *Angew. Chem., Int. Ed.* 37 (1998) 1460.
- [3] O.M. Yaghi, M. O'Keeffe, N.W. Ockwig, H.K. Chae, M. Eddaoudi, J. Kim, *Nature* 423 (2003) 705.
- [4] C.N.R. Rao, S. Natarajan, R. Vaidyanathan, *Angew. Chem., Int. Ed.* 43 (2004) 1466.
- [5] S. Kitagawa, R. Kitaura, S. Noro, *Angew. Chem., Int. Ed.* 43 (2004) 2334.
- [6] G. Férey, *Chem. Soc. Rev.* 37 (2008) 191.
- [7] J.S. Seo, D. Whang, H. Lee, S.I. Jun, J. Oh, Y.J. Jeon, K. Kim, *Nature* 404 (2000) 982.
- [8] M. Eddaoudi, J. Kim, N. Rosi, D. Vodak, J. Wachter, M. O'Keeffe, O.M. Yaghi, *Science* 295 (2002) 469.
- [9] H.K. Chae, D.Y. Siberio-Pérez, J. Kim, Y. Go, M. Eddaoudi, A.J. Matzger, M. O'Keeffe, O.M. Yaghi, *Nature* 427 (2004) 523.
- [10] Y. Liu, G. Li, X. Li, Y. Cui, *Angew. Chem., Int. Ed.* 46 (2007) 6301.
- [11] W. Zhang, R.G. Xiong, S.D. Huang, *J. Am. Chem. Soc.* 130 (2008) 10468.
- [12] A.K. Cheetham, C.N.R. Rao, R.K. Feller, *Chem. Commun.* (2006) 4780.
- [13] O.M. Yaghi, H.L. Li, T.L. Groy, *J. Am. Chem. Soc.* 118 (1996) 9096.
- [14] C. Janiak, *J. Chem. Soc., Dalton Trans.* (2000) 3885.
- [15] J.L.C. Rowsell, O.M. Yaghi, *Micropor. Mesopor. Mater.* 73 (2004) 3.
- [16] S. Leininger, B. Olenyuk, P.J. Stang, *Chem. Rev.* 100 (2000) 853.
- [17] G.F. Sewiegers, T.J. Malefets, *Chem. Rev.* 100 (2000) 3483.
- [18] B. Moulton, M.J. Zaworoto, *Chem. Rev.* 101 (2001) 1629.
- [19] G. Novitchi, W. Wernsdorfer, L.F. Chibotaru, J.P. Costes, C.E. Anson, A.K. Powell, *Angew. Chem., Int. Ed.* 48 (2009) 1614.
- [20] T.C. Stamatatos, A. Vinslava, K.A. Abboud, G. Christou, *Chem. Commun.* (2009) 2839.
- [21] C.D. Ene, F. Tuna, O. Fabelo, C. Ruiz-Pérez, A.M. Madalan, H.W. Roesky, M. Andruh, *Polyhedron* 27 (2008) 574.
- [22] S. Noro, S. Kitagawa, T. Akutagawa, T. Nakamura, *Prog. Polym. Sci.* 34 (2009) 240.
- [23] C.D. Ene, A.M. Madalan, C. Maxim, B. Jurca, N. Avarvari, M. Andruh, *J. Am. Chem. Soc.* 131 (2009) 4586.
- [24] Molecular Structure Corporation, *TEXSAN. Single Crystal Structure Analysis Software*, MSC, 3200 Research Forest Drive: The Woodlands, TX77381, USA, 1995.
- [25] G.M. Sheldrick, *SADABS. Version 2007/2*, Bruker AXS Inc., Madison, Wisconsin, USA, 2007.
- [26] (a) G.M. Sheldrick, *SHELXS97, Program for Solution of Crystal Structures*, University of Göttingen, Göttingen, Germany, 1997.; (b) G.M. Sheldrick, *SHELXL97, Program for Solution of Crystal Structures*, University of Göttingen, Göttingen, Germany, 1997.
- [27] R. Lyszczek, *J. Therm. Anal. Calorim.* 91 (2008) 595.
- [28] Z.H. Sun, W.T. Yu, X.F. Cheng, X.Q. Wang, G.H. Zhang, G. Yu, H.L. Fan, D. Xu, *Opt. Mater.* 30 (2008) 1001.
- [29] Y. Fu, X.Y. Wang, G.B. Li, F.H. Liao, M. Xiong, J.H. Lin, *Chinese J. Inorg. Chem.* 24 (2008) 1224.
- [30] J.H. He, Y.T. Zhang, Q.H. Pan, J.H. Yu, H. Ding, R.R. Xu, *Micropor. Mesopor. Mater.* 90 (2006) 145.
- [31] J.X. Chen, M. Ohba, S. Kitagawa, *Chem. Lett.* 35 (2006) 526.
- [32] X.Y. Wang, H.Y. Wei, Z.M. Wang, Z.D. Chen, S. Gao, *Inorg. Chem.* 44 (2005) 572.
- [33] J. Su, Y.X. Wang, S.H. Yang, G.B. Li, F.H. Liao, J.H. Lin, *Inorg. Chem.* 46 (2007) 8403.
- [34] X.Y. Wang, Z.M. Wang, S. Gao, *Chem. Commun.* (2008) 281.
- [35] G.J.T. Cooper, H. Abbas, P. Kogerler, D.L. Long, L. Cronin, *Inorg. Chem.* 43 (2004) 7266.
- [36] D. Moon, J. Song, B.J. Kim, B.J. Suh, M.S. Lah, *Inorg. Chem.* 43 (2004) 8230.
- [37] M.J. Plater, M.R. St, J. Foreman, E. Coronado, C.J. Gómez-García, A.M.Z. Slawin, *J. Chem. Soc., Dalton Trans.* (1999) 4209.
- [38] S.C. Manna, E. Zangrando, M.G.B. Drew, J. Ribas, N.R. Chaudhuri, *Eur. J. Inorg. Chem.* (2006) 481.
- [39] J. Mroziński, A. Bieńko, P. Kopel, V. Langer, *Inorg. Chim. Acta* 361 (2008) 3723.
- [40] D. Ghoshal, G. Mostafa, T.K. Maji, E. Zangrando, T.H. Lu, J. Ribas, N.R. Chaudhuri, *New J. Chem.* 28 (2004) 1204.
- [41] X.Y. Wang, S.C. Sevov, *Inorg. Chem.* 47 (2008) 1037.
- [42] R.L. Carlin, *Magnetochemistry*, Springer-Verlag, Berlin, 1986, pp. 53–65.
- [43] R.J. Goff, A.J. Williams, J.P. Attfield, *Phys. Rev. B* 70 (2004) 014426.
- [44] M.A.M. Abu-Youssef, M. Drillon, A. Escuer, M.A.S. Goher, F.A. Mautner, R. Vicente, *Inorg. Chem.* 39 (2000) 5022.
- [45] M.E. Fisher, *Am. J. Phys.* 32 (1974) 241.
- [46] D.W. Feng, C. Wang, W.T. Cheng, G.B. Li, S.J. Tian, F.H. Liao, M. Xiong, J.H. Lin, *Solid State Sci.* 11 (2009) 845.
- [47] J.H. Yoon, D.W. Ryu, H.C. Kim, S.W. Yoon, B.J. Suh, C.S. Hong, *Chem.-Eur. J.* 15 (2009) 3661.
- [48] M. Huber, L. Bubacco, M. Beltramini, B. Salvato, H. Elias, J. Peisach, E. Larsen, S.E. Harnung, W. Haase, *Inorg. Chem.* 35 (1996) 7482.
- [49] R.Y. Li, B.W. Wang, X.Y. Wang, X.T. Wang, Z.M. Wang, S. Gao, *Inorg. Chem.* 48 (2009) 7174.